Redox and Spectroscopic Properties of Human Indoleamine 2,3-Dioxygenase and A His303Ala Variant: Implications for Catalysis †

ARTICLE *in* BIOCHEMISTRY · DECEMBER 2005

Impact Factor: 3.02 · DOI: 10.1021/bi0513958 · Source: PubMed

Redox and Spectroscopic Properties of Human Indoleamine 2,3-Dioxygenase and A His303Ala Variant: Implications for Catalysis†

Nektaria D. Papadopoulou,‡ Martin Mewies,‡ Kirsty J. McLean,§ Harriet E. Seward,§ Dimitri A. Svistunenko,|| Andrew W. Munro,§ and Emma Lloyd Raven*,‡

Departments of Chemistry and Biochemistry, University of Leicester, University Road, Leicester, LE1 7RH, United Kingdom, and Department of Biological Sciences, University of Essex, Wivenhoe Park, Colchester, CO4 3SQ, United Kingdom

Received July 18, 2005; Revised Manuscript Received September 5, 2005

ABSTRACT: Indoleamine 2,3-dioxygenase is an important mammalian target that catalyses the oxidative cleavage of L-tryptophan to *N*-formylkynurenine. In this work, the redox properties of recombinant human indoleamine 2,3-dioxygenase (rhIDO) and its H303A variant have been examined for the first time and the spectroscopic and substrate-binding properties of rhIDO and H303A in the presence and absence of substrate are reported. The Fe^{3+}/Fe^{2+} reduction potential of H303A was found to be -30 ± 4 mV; in the presence of L-Trp, this value increases to $+16 \pm 3$ mV. A variety of spectroscopies indicate that ferric rhIDO at pH 6.6 exists as a mixture of six-coordinate, high-spin, water-bound heme and a low-spin species that contains a second nitrogenous ligand; parallel experiments on H303A are consistent either with His303 as the sixth ligand or with His303 linked to a conformational change that affects this transition. There is an increase in the low-spin component at alkaline pH for rhIDO, but this is not due to hydroxide-bound heme. Substrate binding induces a conformational rearrangement and formation of low-spin, hydroxide-bound heme; analysis of the H303A variant indicates that His303 is not required for this conversion and is not essential for substrate binding. The Fe^{3+}/Fe^{2+} reduction potential of H303A variant is ≈70 mV lower than that of rhIDO, leading to a destabilization of the ferrous−oxy complex, which is an obligate intermediate in the catalytic process. In comparison with the properties of other heme enzymes, the data can be used to build a more detailed picture of substrate binding and catalysis in indoleamine 2,3-dioxygenase. The wider implications of these results are discussed in the context of our current understanding of the catalytic mechanism of the enzyme.

The L-kynurenine pathway, which, ultimately, leads to the formation of NAD, is the major catabolic route of L-tryptophan in mammals. The initial, rate-limiting step in this pathway is the oxidative cleavage of L-tryptophan to *N*-formylkynurenine (Scheme 1) and is catalyzed by indoleamine 2,3-dioxygenase (IDO,[1] reviewed in refs *1*−*3*). There is a wealth of evidence linking IDO induction and kynurenine pathway metabolites to various physiological and pathophysiological conditions, including antimicrobial, antiviral, antiparasitic, and antitumor activity, renal allograft rejection, and various neurological disorders (*4*−*8*).

Scheme 1: (A) Reaction Catalyzed by IDO, with IUPAC Numbering Indicated; (B) pH-Dependent Properties of Tryptophan[a]

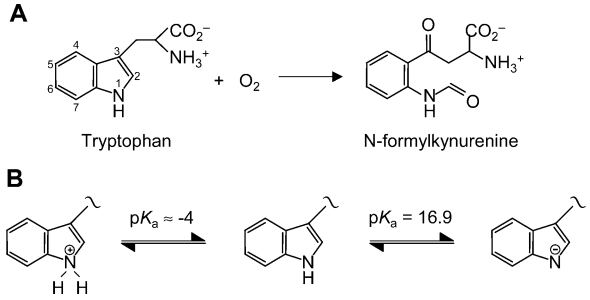

[a] Deprotonation of the NH group of the indole ring occurs with a pK_a of 16.9 (*66*); formation of the doubly protonated species is not favorable [p$K_a \approx -4$ estimated for D-Trp in perchloric acid (*67*)].

IDO is a monomeric, heme-containing enzyme that was first isolated in 1967 (*8*, *9*). It is widely distributed in mammalian tissues. The catalytic mechanism involves reduction of the ferric heme, binding of O_2 to the ferrous heme, and binding of L-Trp, although the precise sequence, O_2 binding followed by L-Trp binding or vice versa, is not known (*10*−*13*). In fact, there is much that we do not understand about this important mammalian target, and there are a number of questions that need urgent attention. There is no crystal structure published; therefore, the nature of the

† This work was supported by The Wellcome Trust (Grant 063688/Z/01/Z to E.L.R.), BBSRC (Studentship to N.P.), University of Essex (Biomedical EPR Facility), and The Royal Society (Leverhulme Trust Senior Research Fellowship to A.W.M.).

* To whom correspondence should be addressed. Telephone: +44-(0)116-228-7047. Fax +44-(0)116-225-3789. E-mail: emma.raven@le.ac.uk.

‡ Department of Chemistry, University of Leicester.

§ Department of Biochemistry, University of Leicester.

|| University of Essex.

[1] Abbreviations: IDO, indoleamine 2,3-dioxygenase; hIDO, human indoleamine 2,3-dioxygenase; rhIDO, recombinant human indoleamine 2,3-dioxygenase; H303A, a site-directed variant of rhIDO in which histidine 303 has been replaced with alanine; EPR, electron paramagnetic resonance; MCD, magnetic circular dichroism; CT, charge transfer; CT_{ls}, low-spin ferric charge-transfer band; CT_1 and CT_2, high-spin ferric charge-transfer bands; SHE, standard hydrogen electrode.

10.1021/bi0513958 CCC: $30.25
Published on Web 10/05/2005

substrate binding and iron−oxygen interactions, the identity of heme active-site residues, and the role of individual residues in catalytic activity and substrate binding are all unknown. In addition, there is no information on the redox properties of the heme for any IDO: this is an important omission because the redox properties of the metal ion are a key determinant in controlling biological function.

To begin to address these deficiencies, we have examined the redox properties (including the influence of substrate on the redox chemistry) and the spectroscopic properties of the substrate-bound and substrate-free IDO. We also present detailed functional data for the H303A variant and an assessment of the likely role of this residue on substrate and dioxygen binding. The results can be used to build a more detailed picture of the possible mechanism of the IDO enzyme, and the collective implications of these results are discussed in terms of our current understanding of the mechanism of IDO catalysis.

EXPERIMENTAL PROCEDURES

Construction of Expression Vector and Bacterial Expression. Construction of the expression vector and expression of rhIDO (*14*, *15*) are described in the Supporting Information.

Mutagenesis. Site-directed mutagenesis was performed using a Quikchange mutagenesis kit (Stratagene) according to the protocol of the manufacturer and confirmed by sequencing the entire IDO-coding region. The PCR product was transformed in Epicurian Coli BL21-Gold (DE3) competent cells (Stratagene) for bacterial expression.

Protein Purification and Handling. The recombinant enzyme is isolated from *Escherichia coli* as the holoenzyme. Cell pellets were resuspended in sonication buffer (50 mM potassium phosphate buffer at pH 8.0 containing 300 mM potassium chloride) containing two EDTA-free Complete tablets (Roche) and stirred with 5 mg of lysozyme for 20 min at room temperature. After 20 min, 5 mg of DNase was added and the suspension was stirred until it became more fluid. The mixture was sonicated on ice using 8 × 30 s bursts from a MSE sonicator. Cell debris was removed by centrifugation (30 min, 20 000 rpm, 8 °C), and the cell-free extract was immediately applied to a 20 mL column of Ni-NTA Superflow resin (Qiagen) previously equilibrated in a sonication buffer. The resin was washed with 100 mL of wash buffer (50 mM potassium phosphate at pH 6.0 containing 300 mM potassium chloride), and the protein was eluted using ∼100 mL of elution buffer (sonication buffer containing 100 mM EDTA). The resulting protein was then exchanged into a storing buffer (50 mM Tris-HCl at pH 7.4 and 1 mM EDTA) and frozen in aliquots at −80 °C. This procedure revealed the presence of only two components (see Figure S2A in the Supporting Information), and electrospray mass spectrometry (not shown) showed two peaks at *m*/*z* 47 170.0 ± 1.8 and 45 643.0 ± 1.7, respectively. The major peak at 47 170.0 corresponds to the calculated mass [*m*/*z* 47 168.22 (*16*, *17*), Figure S1 in the Supporting Information] of the intact protein including the N-terminal His tag; the minor peak corresponds to the calculated mass [*m*/*z* 45 637.48 (*16*, *17*)] of a proteolytically cleaved version of the enzyme (clipped at Lys389). MALDI−TOF analyses (not shown) also gave major (*m*/*z* 47 170 ± 0.24) and minor (*m*/*z* 45 621 ± 0.23) components; proteolytic digestion followed by further MALDI analyses and database searching [MASCOT (Matrixscience Ltd., London, U.K.)] unambiguously identified both fragments as human IDO. Anion-exchange FPLC (AKTA FPLC, Amersham Pharmacia Biotech) using a Mono Q H/R 5/5 column was used to separate the two components (Figure S2B in the Supporting Information). The buffers used were 20 mM Tris-HCl at pH 8.3 and 20 mM Tris-HCl and 1 M NaCl (buffer B). Purified samples of rhIDO isolated in this way had A_{404}/A_{280} of >2.0.[2] Purification of H303A was as described for rhIDO (A_{408}/A_{280} > 1.2). Samples of rhIDO and H303A were exchanged into a storing buffer (50 mM Tris-HCl at pH 7.4 containing 1 mM EDTA) prior to freezing in aliquots at −80 °C.

Absorption coefficients of $\epsilon_{404} = 172$ mM^{-1} cm^{-1} and $\epsilon_{408} = 108$ mM^{-1} cm^{-1} were determined for ferric rhIDO and H303A, respectively, using the pyridine−hemochromagen procedure (*18*). Ferrous rhIDO was generated by the addition of sodium dithionite. The ferrous−oxy derivative was generated either by passing ferrous rhIDO through a 10 mL column of Sepharose G-25 (Amersham Bioscience) equilibrated with O_2-saturated buffer or by direct bubbling of O_2 gas through a dithionite-reduced sample. For rhIDO, both methods gave identical wavelength maxima for the ferrous−oxy derivative. Other ligand-bound derivatives (azide, cyanide, and fluoride) were obtained by the addition of an excess (typically 2−4 μL) of a concentrated (1 M) solution of ligand to the ferric enzyme (typically 5−25 μM) until no further changes in absorbance were observed.

Steady-State Assays. Samples were assayed for catalytic activity in reactions (25.0 °C) that consisted of 10 μM methylene blue (Sigma), 10 μg of catalase (bovine liver, Sigma), 20 mM L-ascorbate (Sigma), and varying concentrations (0−40 μM) of L-Trp contained in 100 mM potassium phosphate buffer (1 mL total volume) (*19*). The reaction was initiated by the addition of rhIDO (10 μL, ∼1 μM). Initial rates were monitored by tracking the increase in the concentration of *N*-formylkynurenine at 321 nm [$\epsilon_{321} = 3.75$ mM^{-1} cm^{-1} (*20*)]. All data were fitted to the Michaelis−Menten equation. pH-dependent data were collected using either 100 mM potassium phosphate as above or glycine−sodium hydroxide buffer.

Electronic Spectroscopy. Electronic absorption spectra (25.0 ± 0.1 °C) were recorded using a Perkin−Elmer Lambda40 UV−vis spectrophotometer. Equilibrium binding constants (μ = 0.05 M) were determined according to published procedures (*21*) using Tris/HCl (pH 8.0−9.5) and phosphate buffers (pH 7.0−8.0). Specifically, this involved preparing samples of protein (≈5−10 μM) and substrate (0.10 M) in the same buffer followed by the addition of small (0.5−2.0 μL) volumes of substrate to the enzyme. Binding constants were determined by monitoring decreases in the absorbance at 406 nm and fitting to eq 1 (*21*)

$$\mathrm{Abs}_{406} = (K_D A_i + [\text{L-Trp}]_{tot} A_f)/(K_D + [\text{L-Trp}]_{tot})$$

[2] Numerous control experiments were carried out on pure mixtures of the intact and cleaved components as well as on FPLC-purified samples of intact rhIDO to determine whether the presence of the minor component affected the catalytic, redox, or spectroscopic properties of the enzyme. We were not able to detect measurable differences in any of the experiments reported in this work.

where A_i and A_f are the initial and final absorbancies, respectively, and $[L\text{-Trp}]_{tot}$ is the total concentration of the substrate.

Magnetic Circular Dichroism (MCD) Spectroscopy. MCD spectra were recorded using Jasco J810 and J730 models for the UV−vis and near-IR regions, respectively. An Oxford Instruments SM-1 superconducting solenoid with a 25 mm room-temperature bore was used to generate a 6 T magnetic field. MCD intensities are linear with respect to the magnetic field at room temperature and are plotted normalized to magnetic field as $\Delta\epsilon/H$ (M^{-1} cm^{-1} T^{-1}). Samples were prepared in deuterated sodium phosphate buffer (50 mM) at the appropriate pH (denoted as pH*) or into the same buffer containing 20 mM L-Trp, to a final concentration of ≈350 μM for vis/near-IR regions and ≈50 μM for the Soret region.

Electron Paramagnetic Resonance (EPR) Spectroscopy. X-Band EPR spectra (10 K) were recorded on a Bruker ER-300D series electromagnet and microwave source interfaced to a Bruker EMX control unit and fitted with an ESR-9 liquid Helium flow cryostat from Oxford Instruments and a dual mode microwave cavity from Bruker (ER-4116DM). Quantification of $S = {}^1/_2$ species was carried out by comparison with the spin standard Cu^{II}(EDTA) using the method of Aasa and Vanngard (*22*). Magnetic field magnitude is detected by a Hall probe within the cavity of the instrument. Additionally, the g values of the Cu^{II}EDTA standard (g = 2.32 and 2.075) were used to ensure the correct field values for the detected frequency (observed values identical to those given above). Frequency is monitored within the EMX unit and also with an additional frequency counter attached to the microwave source.

Electrochemistry. Aneorobic ($[O_2]$ < 2 ppm) redox titrations were performed in a Belle Technology glovebox under nitrogen (*23*). Solutions (100 mM potassium phosphate containing 10% glycerol) of rhIDO (≈4 μM, pH 7.0) or H303A (∼10 μM, pH 8.0) were titrated electrochemically (*24*) using sodium dithionite as a reductant and potassium ferricyanide as an oxidant. Mediators (2 μM phenazine methosulfate, 5 μM 2-hydroxy-1,4-naphthoquinone, 0.5 μM methyl viologen, and 1 μM benzyl viologen) were used to mediate in the range from +100 to −480 mV (*23*, *25*). Data were fitted to the Nernst equation for a single electron process (*26*). Potentials are quoted against the standard hydrogen electrode (SHE).

RESULTS

Characterization of rhIDO.

UV−Vis Spectroscopy. Wavelength maxima for various ferric and ferrous derivatives of rhIDO are given in Table 1. There are no reported wavelength maxima for human IDO (hIDO); we have therefore compared wavelength maxima with the corresponding maxima for the wild-type rabbit enzyme, for which most of the published data have been obtained. Wavelength maxima are similar in most cases, although there are differences in the cyanide and azide derivatives. The spectrum (Figure 1A) of the ferric form of rhIDO (λ_{max} = 404, 500, 535, and 633 nm) has maxima that are consistent with a mixed population of high- and low-spin heme species. Wavelength maxima of 406 and 630 nm for rhIDO have been previously reported (*15*). This spectrum shows no evidence for formation of ahydroxide-bound heme with increasing pH: there are no substantial changes in peak positions or intensities in the pH range of 5.5−10.7 (data not shown), although there is a drop in the Soret band above

Table 1: Absorption Spectra Maxima for Various Ferric and Ferrous Derivatives of rhIDO[a]

	λ_{max} (nm)		
derivative	rabbit IDO[b]	rhIDO[c]	H303A[d]
ferric	406, 500, 534, 570, 632[e]	404, 500, 535, 633	408, 531, 568
ferric + L-Trp	412, 540, 576[e]	411, 540, 576[f]	411, 531, 568
ferrous	429, 558[e]	425, 527[sh], 558	425, 529, 559
ferrous−oxy	415, 544, 577[g]	412, 539, 576[h]	nd[i]
ferrous−CO	420, 539, 570[j]	419, 539, 565	420, 537, 567
ferric−azide	416.5[j]	414, 535, 572, 634	408, 531, 568
ferric−cyanide	428, 532, 562[j]	419, 540, 570[sh]	417, 533, 563
ferric−fluoride	402, 488, 608[j]	404, 497, 537, 572, 632	407, 531, 568

[a] sh = shoulder. [b] Isolated from rabbit intestine. [c] Spectra were run in sodium phosphate at pH 7.0, μ = 0.10 M, and 25.0 °C, except for footnotes *f* and *g* (see below). [d] Spectra were run in 100 mM potassium phosphate at pH 7.9 and 25.0 °C. [e] Taken from ref *13* (at pH 8.0 and 24 °C). [f] These spectra are pH-dependent and were therefore run in sodium phosphate at pH 8.0, μ = 0.10 M, and 25.0 °C for direct comparison with the published spectra (at pH 8.0). [g] Taken from ref *30* (at 4 °C). [h] Spectrum run in sodium phosphate at pH 8.0, μ = 0.10 M, and 25.0 °C. [i] nd = not detectable. [j] Taken from ref *29* (at pH 6.0 and 25 °C).

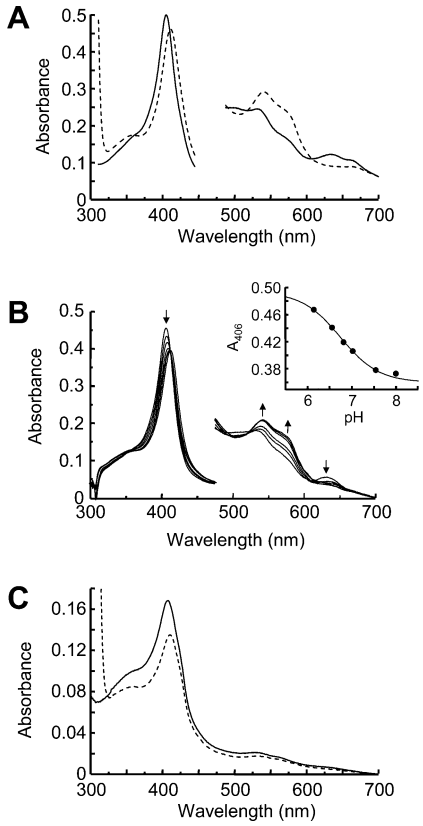

FIGURE 1: (A) UV−vis spectra (pH 8.1 and 25.0 °C) of ferric rhIDO in the absence (—) and presence (- - -) of 20 mM L-Trp. Absorbance values in the visible region have been multiplied by a factor of 5. (B) pH dependence of the UV−vis spectra of rhIDO in the presence of 20 mM L-Trp. (Inset) Fit of the absorbance at 406 nm to a single proton process. Absorbance values in the visible region have been multiplied by a factor of 5. (C) UV−vis spectrum (pH 7.9 and 25.0 °C) of ferric H303A in the absence (—) and presence (- - -) of 20 mM L-Trp.

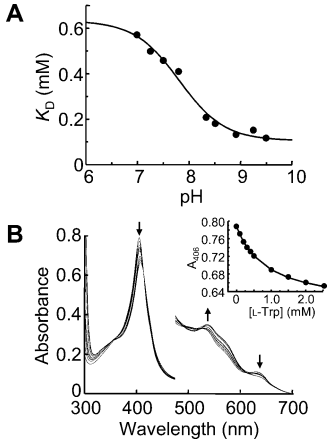

FIGURE 2: (A) Plot of the equilibrium binding constant, K_D, versus pH for binding of L-Trp to rhIDO. Data were fitted to a single proton process. (B) Representative data set for determination of K_D at pH 7.0. The visible region has been multiplied by a factor of 5, and arrows indicate the direction of change in absorbance upon successive additions of L-Trp. (Inset) Fit of data at 406 nm to eq 1 (conditions: 50 mM potassium phosphate at 25.0 °C).

pH ≈8.5. Above pH ≈9 and below pH ≈5, the enzyme was not stable enough to allow meaningful data collection.

Substrate Binding. Binding of L-Trp to ferric rhIDO leads to the formation of a low-spin species (λ_{max} = 411, 540, and 576 nm, Figure 1A). A comparison with other heme proteins [e.g., horseradish peroxidase (pH 12.3), λ_{max} = 414, 543, and 573 nm; horse heart myoglobin (pH 10.9, mixed high spin/low spin), λ_{max} = 411, 485^{sh}, 541, 583, and 593^{sh} nm (*28*)] indicates that the spectrum for rhIDO arises from formation of a low-spin, hydroxide-bound heme. This new substrate-bound species is now pH-dependent (Figure 1B), with low-spin heme dominating at alkaline pH. A pK_a of 6.7 ± 0.1 can be extracted from a plot of the absorbance at 406 nm versus pH (inset of Figure 1B). To quantify the binding interaction, the equilibrium binding constant, K_D, for binding of L-Trp to ferric IDO was measured. At pH 7.0, a value for K_D of 0.57 ± 0.05 mM was determined (not shown). This binding constant varies with pH (Figure 2), indicating that it is sensitive to titration of another group. A fit of these data to a single proton process yields a pK_a of 7.8 ± 0.1.

Steady-State Kinetics. Steady-state oxidation of L-Trp at pH 8.0 gave values for k_{cat} and K_M of 5.2 ± 0.2 s^{-1} and 7.1 ± 1.1 μM, respectively (k_{cat}/K_M = 0.73 μM^{-1} s^{-1}). Steady-state data for rhIDO have been reported (*14*) (but no k_{cat} was reported). There is no reported k_{cat} for hIDO; K_M has been previously reported as ≈20 μM (*19*) and 18 μM (*27*) for hIDO.

MCD Spectroscopy (Ferric rhIDO at Acidic and Alkaline pH). UV−vis and near-IR MCD spectra of rhIDO at pH 6.6 (Figure 3A and 3B, respectively) are characteristic of ferric heme, showing both low- and high-spin features. MCD spectra for rabbit IDO have been published previously (*29*, *30*), but did not include measurements in the near-IR region from which very detailed information can be obtained. For rhIDO, the Soret crossover is at 410 nm and its peak-trough intensity is between the values expected for a purely low-spin (120−160 M^{-1} cm^{-1} T^{-1}) or high-spin (5−25 M^{-1} cm^{-1} T^{-1}) species (*31*). Low-spin bands dominate the visible region, but a negative feature at 641 nm is part of a high-

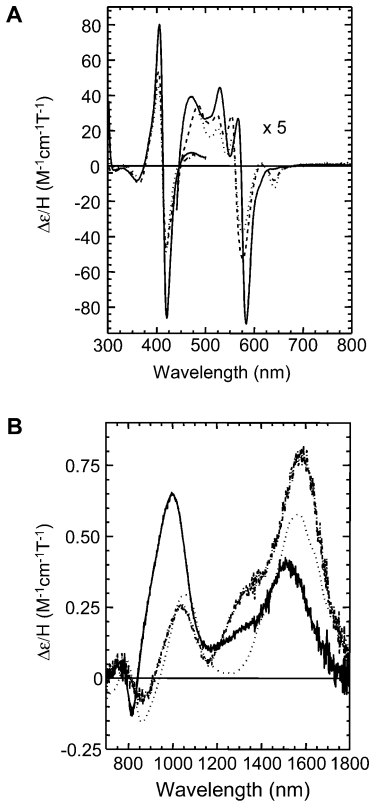

FIGURE 3: Room-temperature MCD at 6 T in the UV−vis (A) and near-IR (B) regions of ferric rhIDO at pH* 6.6 (•••, [rhIDO] = 132 μM in both cases), ferric rhIDO at pH* 8.0 (- - -, [rhIDO] = 35 and 169 μM in the Soret and vis/near-IR, respectively), and ferric rhIDO at pH* 8.0 in the presence of 20 mM L-Trp (—, [rhIDO] = 45 and 224 μM, respectively).

spin ligand−metal charge-transfer derivative, CT_2. Spectra in the near-IR region (Figure 3B) are also consistent with a mix of high- and low-spin species. In this case, two CT bands are observed at 1040 and 1570 nm. The 1570 nm band arises from ligand−metal charge transfer from the porphyrin to the ferric d orbitals of low-spin iron (CT_{ls}), and its position is consistent with bisnitrogenous ligation (*32*, *33*). The MCD spectra of high-spin heme species also contain ligand−metal CT bands, CT_1 and CT_2, which shift with changes in the axial ligation (*28*, *34*). The CT_2 band is observed as the negative trough of the derivative in the visible region (see above). The feature at 1040 nm is the positive lobe of the CT_1 derivative, and the negative lobe of this band is obscured by the more intense CT_{ls} band at 1570 nm. This negative lobe obscures in turn with the vibrational sideband of the CT_{ls} feature. Together, the positions of $CT_{1,2}$ are consistent with coordination of a nitrogen ligand and a second, neutral ligand to the heme (e.g., histidine/water). The intensities of the transitions suggest roughly equal populations of high- and low-spin heme at this pH.

At pH 8.0 (Figure 3), there is an increase in intensity in the Soret and visible regions, reflecting an increase in low-spin heme content, and a decrease in the CT_2 band (641 nm), reflecting a decrease in high-spin heme content. In the near-IR region, the 1040 nm feature has decreased to a similar extent (15% of total heme population) and the more intense CT_{ls} feature at 1570 nm now has a vibrational sideband at 1346 nm. There are no major changes in wavelength maxima of the CT bands compared to pH 6.6, which suggests that the two dominant species observed at acidic pH (low-spin

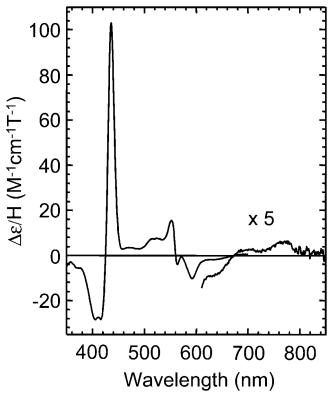

FIGURE 4: Room-temperature MCD spectra at 6 T of ferrous rhIDO (66 μM) at pH* 6.6.

bisnitrogenous and high-spin histidine/water) are unchanged. In contrast to previous work (*35*), there is no evidence at room temperature for the formation of a histidine/hydroxide species at alkaline pH, in agreement with the observation (*vide supra*) that the UV−vis spectrum of rhIDO is pH-independent. Histidine/hydroxide coordination is characteristic of intense $CT_{1,2}$ bands, which are shifted to a lower wavelength compared to histidine/neutral ligand species (*28*, *34*, *36*).

MCD Spectroscopy (Ferric rhIDO + L-Trp). In the presence of L-Trp at pH 8.0, there is a clear increase in intensity throughout the Soret and visible regions, which indicates an increase in low-spin heme. The high-spin CT_2 band at 641 nm (Figure 3A) is diminished in intensity and accounts for only ≈7% of the total heme species. There are shifts in the bands throughout the visible region that indicate formation of a new low-spin species; this is confirmed in the near-IR spectrum, where a new feature at 1000 nm is observed. The shift in peak wavelength from the position of the CT_1 positive lobe, the absence of a corresponding CT_2 band in the visible region, and the clear vibrational sideband in the second CT_{ls} feature suggest that this band is a CT_{ls} feature arising from a new low-spin species rather than from a feature of a high-spin CT_1 band. Its maximum at 1000 nm is similar to that observed for hydroxide-bound myoglobin (1035 nm) (*28*, *37*) and hydroxide-bound horseradish peroxidase at pH 12.3 (1100 nm) (*38*, *39*), both of which have histidine/hydroxide ligation at room temperature. The second CT_{ls} feature at 1515 nm is shifted by ∼60 nm from its maximum in the absence of tryptophan but remains in the range expected for histidine/nitrogenous axial ligation, and there are no changes in the corresponding EPR species (g_z = 2.94, *vide infra*) upon binding of L-Trp, which suggests no major changes in the ligation or ligand conformation in this species. The intensity of this band accounts for ≈30% of the heme population.

MCD Spectroscopy (Ferrous rhIDO). The spectrum of ferrous rhIDO (Figure 4) contains an asymmetric Soret feature with a positive peak at 436 nm, positive features at 524, 552, and ∼770 nm, and negative features at 532 and 592 nm. The spectrum is similar to ferrous myoglobin (*40*, *41*) and ferrous horseradish peroxidase (*42*), both of which contain five-coordinate, high-spin heme. We therefore assign ferrous rhIDO as containing a five-coordinate high-spin heme as the single species, with histidine as the fifth (proximal) ligand. There is no evidence for low-spin heme, which

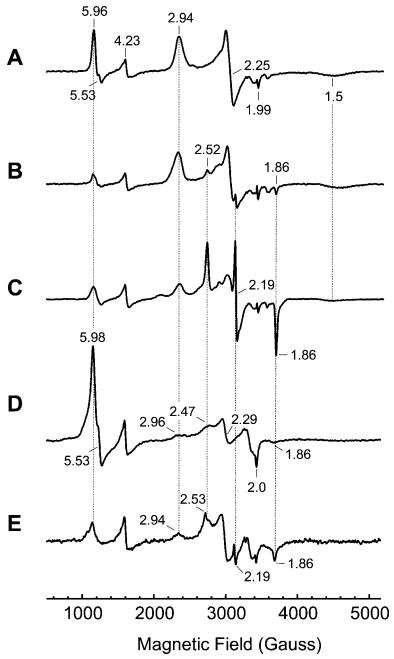

FIGURE 5: Perpendicular mode X-band EPR spectra of ferric rhIDO at pH 6.6 (A), ferric rhIDO at pH 8.0 (B), ferric rhIDO in the presence of 20 mM L-Trp at pH 8.0 (C), ferric H303A at pH 7.5 (D), and ferric H303A in the presence of 20 mM L-Trp at pH 7.5 (E). Conditions: microwave frequency, 9.67 GHz; microwave power, 2 mW; modulation amplitude, 10 G; temperature, 10.8 K; scan speeds and time constants are the same for all spectra. Spectra have been adjusted for differences in the enzyme concentration and receiver gain where required. Gains were typically of the order of 2×10^5−8×10^5.

suggests that any internal (nitrogenous) ligands present in the ferric form are no longer coordinated.

EPR Spectroscopy. EPR spectra for human IDO have not been published, although rabbit IDO has been examined (*29*). The EPR spectrum of rhIDO at pH 6.6 (Figure 5A) contains high- and low-spin species with g values of g = 5.96, 5.53, and 1.99 and g = 2.94, 2.25, and 1.50, respectively.[3] Rhombic g values of 2.94, 2.25, and 1.50 are associated with bishistidine ligation, in which the histidine planes are near parallel (*33*, *43*, *44*). The high-spin signals are slightly rhombic with splitting on the g_{xy} feature at g = 5.7.

At pH 8.0 (Figure 5B), the high-spin signals are diminished with respect to the low-spin species, with the latter accounting for ≈80% of the heme population at 10.8 K. Minor but sharp features at g = 2.52 and 1.86 (middle g value obscured) represent a low-spin species whose g values are consistent with those seen in histidine/hydroxide coordination: because there is no evidence of histidine/hydroxide coordination in the MCD spectra at room temperature (as discussed above, Figure 3), this probably reflects a freezing-induced artifact. There are numerous examples in the heme literature (particularly the peroxidase literature, see for example ref *45*) of water/histidine-coordinated heme producing a fraction of low-spin heme species at cryogenic temperatures for which there is no evidence at room temperature. The factors that influence this are not known.

[3] A minor feature (g = 4.23) is commonly observed for heme proteins and represents high-spin adventitious iron. The splitting on the $g \approx 6$ feature is unusual for six-coordinate (His/H_2O) ligation and may be due to small amounts of buffer-derived phosphate binding to the heme under cryogenic conditions.

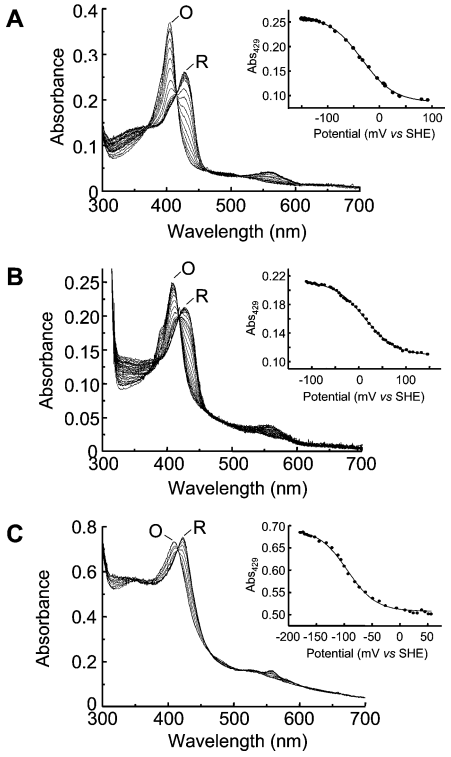

FIGURE 6: (A) Selected absorption spectra obtained during redox titration of rhIDO at pH 7.0. The fully oxidized (O) and fully reduced (R) spectra are indicated. The inset shows a plot of the absorbance at 429 nm against the potential. The solid line is a fit of the data to the Nernst equation for a single electron process. Essentially identical results were obtained by fitting the data at 410 nm. (B) Similar set of absorption spectra collected during redox titration of the substrate-bound form of rhIDO at pH 7.0. The inset shows a plot of absorbance data at 429 nm against the potential, with the corresponding Nernst fit. Fits of the data at 410 nm produced a virtually identical midpoint potential. (C) Redox titration of H303A at pH 8.0, with a fit of the data at 429 nm to the Nernst equation shown in the inset.

Upon addition of L-Trp at pH 8.0, sharp rhombic signals ($g = 2.52$, 2.19, and 1.86) are observed (Figure 5C) that arise from low-spin heme and are associated with histidine/hydroxide coordination. Minor signals from high-spin heme ($g = 5.96$) and the other low-spin species ($g_z = 2.94$) are also present in this spectrum.

Redox Potentiometry. Selected spectra obtained during anaerobic redox titration of rhIDO are shown in Figure 6A. The redox process was clearly reversible, with no sign of hysteresis in the oxidative or reductive directions; spectra collected in the oxidative and reductive stages were near identical at equivalent potentials. Clean isosbestic points were observed, indicating only two absorbing species. Control experiments confirmed that the observed reduction potential was not altered in the presence of the minor (cleaved) component. Upon reduction of rhIDO, there is a decrease in intensity of the Soret band and a shift to a longer wavelength, consistent with the formation of ferrous heme (Table 1). Data were fitted to a single electron process (Nernst equation) at either 407 nm (not shown) or 429 nm (inset of Figure 6A); these analyses at different wavelengths gave results that were within error of one another. The reduction potential (average value from data at 407 and 429 nm) was -30 ± 4 mV.

In the presence of 15 mM L-Trp (Figure 6B), similar absorbance changes were observed. In this case, the reduction potential was 16 ± 3 mV (inset of Figure 6B), an increase of 46 mV over the value for the substrate-free enzyme.

Characterization of the H303A Variant.

On the basis of sequence comparisons with IDO-like myoglobins (*46*), IDO is proposed to contain both proximal [assigned as His346 (*14*)] and distal histidine residues. In the absence of crystallographic information, the highly conserved His303 residue is believed to be located near the heme distal pocket.

Electronic and EPR Spectroscopy. The UV−vis spectrum of ferric H303A[4] ($\lambda_{max} = 408$, 531, 568 nm, Figure 1C and Table 1) shows that the Soret band has red-shifted compared to rhIDO but is still characteristic of high-spin heme. This spectrum is pH-independent, as observed for rhIDO. The spectrum of ferrous H303A is essentially identical to that of rhIDO (Table 1). Cyanide binds to H303A, as evidenced by the change in the electronic spectrum and its similarity to that of rhIDO. There is a decrease in intensity of the Soret band upon addition of azide to H303A but no corresponding changes in the visible region that indicate formation of the expected low-spin heme. Upon binding of L-Trp at pH 8.0 (Figure 1C), the Soret band shifts to a value ($\lambda_{max} = 411$ nm) that is characteristic of low-spin heme formation and that is similar to that observed for rhIDO, but in the visible region, there is no measurable change as observed for rhIDO. EPR analyses indicate that the ferric derivative (Figure 5D) has a much higher proportion of high-spin heme ($g = 5.98$, 5.53, and 2.00) than for rhIDO. Significantly, the low-spin signals arising from the low-spin, bisnitrogenous species ($g = 2.96$, 2.29, and 1.50) are very considerably diminished (the very weak signal that does remain probably arises from coordination of another strong field ligand). The low-spin signals ($g = 2.47$, 2.19, and 1.86) associated with hydroxide ligation in rhIDO are broader for H303A, which suggests the presence of a range of conformers. Addition of L-Trp (Figure 5E) leads to an increase in low-spin heme at $g = 2.53$, 2.19, and 1.86: these sharp signals are consistent with a hydroxide-bound heme species that is in a defined conformation, rather than a range as observed above. An MCD spectrum of H303A could not be obtained because the sample was unstable during repeated exchange into D_2O.

Steady-State Kinetics. The H303A variant was observed to be capable of steady-state oxidation of L-Trp at pH 8.0 under conditions identical to those used for rhIDO, with values for k_{cat} and K_M of 2.7 ± 0.1 s^{-1} and 15 ± 1.0 μM, respectively ($k_{cat}/K_M = 0.18$ μM^{-1} s^{-1}). This is in agreement with previous steady-state analyses on the H303A variant (*14*).

Redox Potentiometry. Selected spectra obtained during redox titration of H303A are shown in Figure 6C. Data obtained at 423 nm (to monitor formation of ferrous heme) were fitted to a single electron process (Nernst equation) and gave a reduction potential of -99 ± 2 mV, representing a destabilization of the ferrous heme of almost 70 mV compared to rhIDO.

Formation of Ferrous−Oxy Derivative. To check whether this decrease in reduction potential was functionally significant, we tested whether destabilization of the ferrous derivative may affect stability of the catalytic ferrous−oxy

[4] The H303A variant has been prepared previously (*14*), but no detailed spectroscopic or redox analyses were presented.

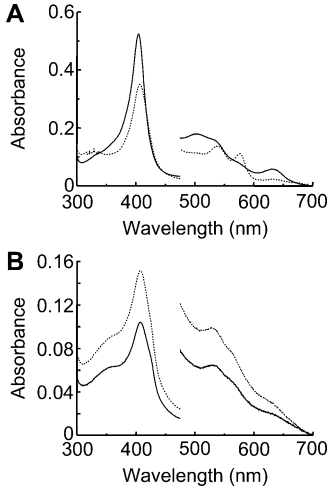

FIGURE 7: UV−vis spectra (100 mM potassium phosphate at pH 7.9 and 25.0 °C) of the ferric (—) and ferrous−oxy (···) derivatives of rhIDO (A) and H303A (B). Absorbance values in the visible region have been multiplied by a factor of 5.

intermediate. Under conditions that resulted in clean formation of the ferrous−oxy complex for rhIDO (see the Experimental Procedures), formation of the ferrous−oxy complex for H303A was not observed. Hence, for rhIDO, a species with wavelength maxima of 412, 539, and 576 nm (Figure 7 and Table 1) was obtained: these maxima are in the range expected for ferrous−oxy heme [e.g., 418, 543, and 581 nm for sperm whale myoglobin (*18*)]. The identical experiment with H303A gave no characteristic oxy peaks in the visible region and no shift in the Soret maximum (Figure 7). In separate rapid-scanning stopped-flow experiments (not shown), no further evidence for transient formation of a ferrous−oxy complex was obtained. Attempts to increase the yield of the ferrous−oxy derivative by addition of imidazole (to 10 mM),[5] which has been shown to recover hydrogen-bonding interactions with bound ligands (*47*), were unsuccessful.

DISCUSSION

Development of our understanding of the detailed mechanism of the IDO enzyme has been hampered by the limited quantities of pure enzyme that can be extracted and purified from readily available sources. For the human enzyme, there is very little functional or spectroscopic information available (*14*, *35*, *46*, *48*, *49*). In this work, we have developed an efficient bacterial expression system for production of hIDO and have used this to examine the redox, spectroscopic, and substrate-binding properties of the enzyme. In this section, the major findings are discussed in the context of our current understanding of the nature of the heme environment, the mechanism of substrate binding, and the redox properties of the IDO enzyme.

Heme Coordination Environment. A summary of the various species present in solution for ferric rhIDO at different pHs and in the presence and absence of the substrate is given in Table 2. Overall, the electronic, MCD, and EPR spectra at acidic pH are clearly consistent with the presence of two distinct species in solution: a high- and low-spin heme

Table 2: Distribution of Heme Species in Ferric rhIDO at Different pH Values in the Presence and Absence of Substrate, as Determined from MCD[a] and EPR Analyses[a]

proximal/ distal ligand	−Trp (%)		+Trp (%)
	pH 6.6	pH 8.0	pH 8.0
His/H_2O (HS)	50	35	7
His/X (LS)	50	65	33
His/OH^- (LS)	nd	nd	60

[a] HS = high-spin heme; LS = low-spin heme; nd = not detected. The percentages stated are derived from MCD intensities, and errors on percentages are estimated as ±5%. Spectra are quantified with the reference to well-characterized model systems [e.g., myoglobin and its complexes and other low-spin compounds (*65*)]. As a guide, a typical high-spin intensity for 100% population of histidine-bound heme is 1 M^{-1} cm^{-1} T^{-1} (peak−trough intensity) and for 100% population of low-spin histidine-ligated heme is between 0.8 and 1.2 M^{-1} cm^{-1} T^{-1} (peak maximum).

species in approximately equal population. The high-spin species is confirmed by MCD as arising from histidine/water ligation. Similar conclusions were reached using resonance Raman spectroscopy (*35*), and His346 has been assigned as the (proximal) ligand in this case (*14*). The low-spin species, which has been observed previously (*29*, *35*), is assigned by MCD as being consistent with bisnitrogenous ligation. Hydroxide ligation, as previously proposed (*35*), is ruled out by the MCD analyses. The identity of the sixth ligand has been a matter of ongoing speculation in the literature (reviewed in ref *1*). EPR data for the H303A variant are useful in this context and are consistent with two possible interpretations: either that His303 is the sixth nitrogenous ligand in this low-spin species or that His303 is located in a region of the protein that is (indirectly) involved in controlling a larger conformational change within the protein structure that leads to formation of this low-spin derivative. It is not known, at this stage, whether the high- and low-spin components are in equilibrium with one another and, if so, on what time scale this occurs. If they are in equilibrium, then a conformational rearrangement of the protein structure would presumably be necessary for the two forms to interconvert (and the fact that significant changes in iron coordination geometry occur upon binding of the substrate indicate that conformational changes of this kind are realistic).[6]

The electronic spectrum of ferric rhIDO is pH-independent, indicating that the distal water molecule does not titrate within the experimentally accessible pH range (pH 5.5−10.7 in our experiments). This is in contrast to the related tryptophan 2,3-dioxygenase enzyme (which catalyses the same reaction as IDO), in which the electronic spectrum is pH-dependent (*52*). The electronic spectra are consistent with the MCD data, which clearly indicate that there is essentially no hydroxide-bound heme at either pH 6.6 or 8.0. There is an increase in low-spin heme at pH 8.0, but this is due to an increase in the bishistidine species and not to the formation of hydroxide-bound heme. An increase in the low-spin component at alkaline pH has also been observed by resonance Raman and assigned as hydroxide-bound heme (*35*). Our data show that this assignment is incorrect, which

[5] Imidazole was not observed to bind to ferric H303A under these conditions (as evidenced by UV−vis spectroscopy).

[6] This is not the only example of a heme protein with mixed coordination geometry. Other examples include leghemoglobin (*50*) and cytochrome *c* at alkaline pH (*51*).

would explain the reported (*35*) failure to detect any ν_{Fe-OH^-} stretching frequency at alkaline pH.

Substrate Binding. MCD and EPR spectra confirm that the predominant species present in the substrate-bound form of rhIDO is hydroxide-bound heme. This is consistent with resonance Raman spectra for the substrate-bound derivative of human IDO (*35*) and previous MCD/EPR spectra for rabbit IDO (*29*). In contrast to the ferric enzyme (*vide supra*), the spectrum of this substrate-bound species is now pH-dependent and a pK_a of 6.7 was derived (Figure 1B). The spectroscopic changes reflect titration of an ionisable residue that affects binding of L-Trp, which explains the appearance of high-spin signals at acidic pH (weaker binding at acidic pH). The pH dependence of the binding interaction can also be determined separately by measuring the change in K_D with pH (Figure 2; pK_a = 7.8). The two pK_a values are in reasonable agreement and are assumed, but not unambiguously confirmed to report, on the same process. This is discussed in more detail below.

A comparison of the pH-dependent properties of substrate-free and substrate-bound rhIDO provides new information that is particularly informative in terms of our understanding of the substrate-binding process. The fact that the spectrum of ferric rhIDO shows no evidence for formation of a hydroxide-bound heme is an unexpected observation in view of the fact that several other heme proteins with known histidine/water coordination, including the closely related tryptophan 2,3-dioxygenase enzyme, have titratable distal water molecules [e.g., myoglobin (*18*), leghemoglobin (*53*), and cytochrome *c* peroxidase (*54*, *55*)]. A conveniently positioned hydrogen-bond acceptor, usually but not exclusively the distal histidine residue, is the normal way in which deprotonation of the bound water is facilitated. Why, then, does the distal water molecule in ferric rhIDO not titrate in a similar manner? The most reasonable explanation is that, in the absence of the substrate, there is no suitable hydrogen-bond acceptor able to stabilize hydroxide formation.[7] (We note that Terentis et al. (*35*) have proposed a direct hydrogen bond between the distal histidine and the distal water molecule in ferric IDO, but this is only consistent with the pH-independent spectrum of the ferric form if the pK_a of the bound water is unaffected by the hydrogen bond or if it is lowered to such an extent as to still be outside the accessible pH range.) The fact that pH-dependent behavior is observed in the tryptophan-bound form presumably means that substrate binding induces a conformational change within the overall protein structure that favors deprotonation, such that a suitable (pH-dependent) hydrogen-bond acceptor is now accessible. One possible scenario that accounts for our observed data is depicted in Scheme 2. Here, the binding of the substrate leads to a hydrogen-bonding interaction between an unspecified active-site acid/base group, the bound substrate, and the distal water molecule. In the absence of the substrate (Scheme 2, left), no such hydrogen-bonding interaction occurs. This would be consistent with the pH-dependent spectrum of the substrate-bound enzyme and the pH dependence of L-Trp binding, because L-Trp can now act as a proton donor/acceptor, shuttling a proton between the distal water molecule and the acid/base group. The pH dependencies observed in this work would therefore be assigned as arising from the titration of one of the residues indicated in Scheme 2, but we cannot unambiguously assign these pK_a values at this stage.[8]

Scheme 2: Proposed Mechanism for Substrate Binding and Hydrogen-Bond Formation in IDO[a]

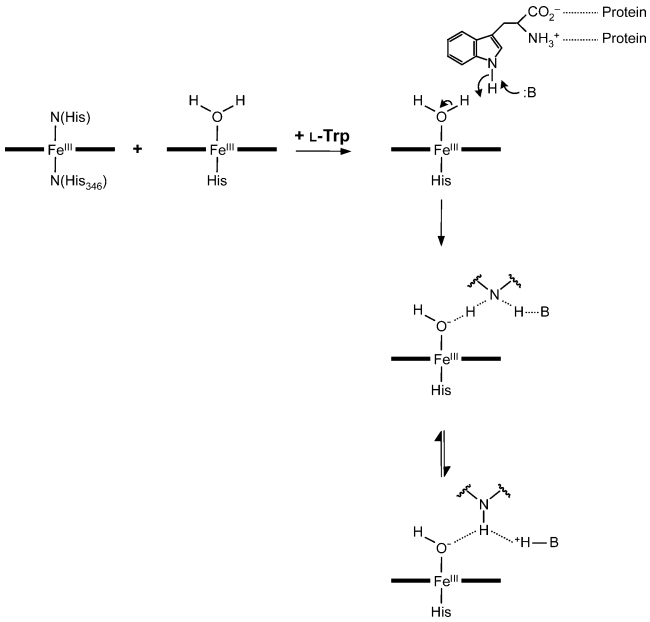

[a] Ferric rhIDO is represented as a mixture of high-spin (water-bound) and low-spin (proposed as histidine-bound) species. Deprotonation of the distal water molecule is induced on substrate binding by favorable hydrogen-bond interactions between the substrate and an active-site acid/base group (the latter only being accessible in the presence of the substrate). Unspecified hydrogen-bonding interactions between the carboxylate and amine groups of the side chain of L-Trp and the protein are also envisaged. Note that the chemistry of the indole ring does not *require* an active-site base to be present for catalysis, because electrophilic addition to the indole ring is possible in the absence of a base.

The fact that H303A is catalytically competent for L-Trp turnover suggests that substrate binding is not critically dependent upon the presence of this residue. This is in agreement with the EPR data for the H303A variant because H303A is observed by EPR to form a low-spin, hydroxide-bound heme upon addition of the substrate. These results clearly indicate that deprotonation of the distal water molecule can occur in H303A and are interpreted as indicating either that His303 does not act as the acid/base acceptor in the wild-type protein or that an alternative proton-transfer mechanism is available in this variant.

Redox Properties and Dioxygen Binding. Table 3 collates the redox data obtained in this work. The reduction potential of IDO has not been previously reported. The magnitude of the observed potential for rhIDO (-30 ± 4 mV) is useful in

[7] This would, necessarily, also have to include the sixth ligand to the heme in the low-spin form which, although it ligates to the heme, must also be unable to induce deprotonation of the bound water molecule in the absence of the substrate. As we have mentioned above, it is likely that conformational changes in the protein structure are involved, such that mobile residues may move in and out of the active-site pocket.

[8] Clearly, the pK_a values of the groups involved need to be in a similar range for proton shuttling to occur. We note that the relevant pK_a values of free L-Trp are out of the physiological range (Scheme 1) but that shifts in the pK_a values could occur upon binding to the enzyme. Formally, however, Scheme 2 does not require complete deprotonation or protonation of L-Trp: we envisage a "concerted" process.

Table 3: Summary of Fe^{3+}/Fe^{2+} Reduction Potentials Obtained in This Paper (Refer to Figure 6)

enzyme	−Trp (mV)	+Trp (mV)
rhIDO	-30 ± 4^a	16 ± 3^a
H303A	-99 ± 2^b	nd[c]

[a] pH 7.0. [b] pH 8.0. [c] nd = not determined.

a functional context. It is lower than those observed in the myoglobins ($E° \approx +50$ mV (reviewed in ref *56*), in which stabilization of the ferrous−oxy complex is required, but is higher than those observed in the heme peroxidases [$E°$ typically in the range from −100 to −250 mV (*57*−*63*)], in which charge separation of the O−O peroxide bond and stabilization of the high-valent ferryl intermediate is required. In the peroxidases, there is a strong hydrogen bond between the proximal histidine and an aspartic acid group: this stabilizes the ferryl intermediate and drives the potential down. Charge separation is not necessary in the globins: in this case, there is no strong hydrogen bond and a higher reduction potential, favoring ferrous heme, is observed. Using resonance Raman techniques, Terentis et al. (*35*) have suggested a strong hydrogen-bonding partner to the proximal ligand in IDO, analogous to the proximal Asp residue in the heme peroxidases, although in this case, the identity of the hydrogen-bonding partner is not known [Asp274 has been suggested, however (*14*)]. On the basis of comparisons with the reported reduction potentials for the peroxidases, the potential for rhIDO is substantially higher than would be expected if a strong hydrogen bond from His346 really does exist.

Upon binding of the substrate, there is a 46 mV increase in reduction potential for rhIDO, reflecting additional stabilization of the ferrous derivative. This increase has not been reported previously and is analogous to but less than the corresponding increase in reduction potential (∼130−140 mV) observed in both cytochrome $P450_{cam}$ (*64*) and P450 BM3 (*26*) upon binding of substrates (camphor and fatty acids, respectively). For P450, this large increase in reduction potential acts as a switch, to turn on electron transfer to the ferric heme. For IDO, it is not clear at this stage whether heme reduction precedes substrate binding or vice versa, but a thermodynamic stabilization of the reduced form would clearly favor catalytic reduction prior to substrate binding. We note, however, that the potentials of substrate-free and substrate-bound forms of IDO are more positive than their P450 counterparts (potentials typically in the range from −350 to −400 mV for substrate-free P450s and from −200 to −250 mV for the substrate-bound forms); perhaps, with its higher potential, IDO does not need to depend upon a substrate-induced mechanism for stabilization of catalytically active ferrous heme.

For the H303A variant, there is considerable (≈70 mV) destabilization of the reduced form compared to the wild-type protein. This brings the potential for this variant into the range expected for a heme peroxidase (in which the ferrous form is considerably destabilized). The functional implication of this decrease in potential is clear: the catalytic ferrous−oxy derivative is now too unstable to be detected under conditions that allow its detection in the wild-type protein. A binding orientation for dioxygen in which His303 influences the hydrogen-bonding structure of the bound ligand would be consistent with this observation.

Clearly, there are many questions that remain to be answered, but these data help to build a more informed picture of the detailed mechanism of IDO catalysis and provide a useful and testable framework for further structure/function studies on this important mammalian target.

ACKNOWLEDGMENT

We thank Dr. Sohan Gupta (Hipple Cancer Research Center) for the gift of the IDO cDNA and Professor Andrew Thomson and Dr. Myles Cheesman (University of East Anglia) for the use of EPR/MCD facilities. We are grateful to Dr. Christof Lenz (Applied Biosystems) for MALDI−TOF analyses, Mr. Kuldip Singh for technical assistance, and Dr. Bernard Rawlings (University of Leicester) and Professor Chris Cooper (University of Essex) for insightful discussions.

SUPPORTING INFORMATION AVAILABLE

The construction of the expression vector, mutagenesis/bacterial expression of recombinant IDO, and protein purification; nucleotide sequence of human IDO (Figure S1); (A) SDS−PAGE gel of a sample of rhIDO prior to FPLC analysis, showing molecular weight markers (left), (B) SDS−PAGE gel of a purified sample of rhIDO after FPLC (Figure S2). This information is available free of charge via the Internet at http://pubs.acs.org.

REFERENCES

1. Sono, M., Roach, M. P., Coulter, E. D., and Dawson, J. H. (1996)-Heme-containing oxygenases, *Chem. Rev. 96*, 2841−2887.
2. Hayaishi, O, T. O., and Yoshida, R. (1990) Indoleamine 2,3-dioxygenase: Properties and functions of a superoxide utilizing enzyme, *Prog. Inorg. Chem. 38*, 75−94.
3. Thomas, S. R., and Stocker, R. (1999) Redox reactions related to indoleamine 2,3-dioxygenase and tryptophan metabolism along the kynurenine pathway, *Redox Rep. 4*, 199−220.
4. Kerr, S. J., Armati, P. J., Pemberton, L. A., Smythe, G., Tattam, B., and Brew, B. J. (1997) Kynurenine pathway inhibition reduces neurotoxicity of HIV-1-infected macrophages, *Neurology 49*, 1671−1681.
5. Grohmann, U., Fallarino, F., and Pucceti, P. (2003) *Trends Immunol. 24*, 242−248.
6. Aquilina, J. A., Carver, J. A., and Truscott, R. J. W. (1997) *Exp. Eye Res. 64*, 727−735.
7. Munn, D. H., Zhou, M., Attwood, J. T., Bondarev, I., Conway, S. J., Marshall, B., Brown, C., and Mellor, A. L. (1998) Prevention of allogeneic fetal rejection by tryprophan catabolism, *Science 281*, 1191−1193.
8. Yamamoto, S., and Hayaishi, O. (1967) Tryptophan pyrrolase of rabbit intestine, *J. Biol. Chem. 242*, 5260−5266.
9. Higuchi, K., and Hayaishi, O. (1967) Enzymic formation of D-kynurenine from D-tryptophan, *Arch. Biochem. Biophys. 120*, 397−403.
10. Taniguchi, T., Sono, M., Hirata, F., Hayaishi, O., Tamura, M., Hayashi, K., Iizuka, T., and Ishimura, Y. (1979) Indolemine 2,3-dioxygenase−Kinetic studies on the binding of superoxide anion and molecular oxygen to enzyme, *J. Biol. Chem. 254*, 3288−3294.
11. Sono, M. (1990) Spectroscopic and equilibrium studies of ligand and organic substrate binding to indoleamine 2,3-dioxygenase, *Biochemistry 29*, 1451−1460.
12. Sono, M. (1986) Spectroscopic and equilibrium properties of the indoleamine 2,3-dioxygenase tryptophan O-2 ternary complex and of analogous enzyme derivatives−Tryptophan binding to ferrous enzyme adducts with dioxygen, nitric oxide, and carbon monoxide, *Biochemistry 25*, 6089−6097.

13. Sono, M., Tanigushi, T., Watanabe, Y., and Hayaishi, O. (1980) Inoleamine 2,3-dioxygenase—Equilibrium studies of the tryptophan binding to the ferric, ferrous, and CO-bound enzymes, *J. Biol. Chem. 255*, 1339−1345.
14. Littlejohn, T. K., Takikawa O., Truscott, R. J. W., and Walker, M. J. (2003) Asp^{274} and His^{346} are essential for heme binding and catalytic function of human indoleamine 2,3-dioxygenase, *J. Biol. Chem. 278*, 29525−29531.
15. Littlejohn, T. K., Takikawa O., Skylas, D., Jamie, J. F., Walker, M. J., and Truscott, R. J. W. (2000) Expression and purification of recombinant human indoleamine 2,3-dioxygenase, *Protein Expression Purif. 19*, 22−29.
16. http://ca.expasy.org/tools/peptide-mass.html.
17. Dai, W., and Gupta, S. L. (1990) Molecular cloning, sequencing, and expression of human interferon-γ-inducible indoleamine 2,3-dioxygenase cDNA, *Biochem. Biophys. Res. Commun. 168*, 1−8.
18. Antonini, M., and Brunori, E. (1971) *Hemoglobin and Myoglobin and Their Reactions with Ligands*, North-Holland Publishers, Amsterdam, The Netherlands.
19. Takikawa, O., Kuroiwa, T., Yamazaki, F., and Kido, R. (1988) Mechanism of interferon-γ action, *J. Biol.* Chem. *263*, 2041−2048.
20. Shimizu, T., Nomiyama, S., Hirata, F., and Hayaishi, O. (1978) Indoleamine 2,3-dioxygenase—Purification and some properties, *J. Biol. Chem. 253*, 4700−4706.
21. Patel, N., Jones, D. K., and Raven, E. L. (2000) Investigation of the haem−nicotinate interaction in leghaemoglobin: Role of hydrogen bonding, *Eur. J. Biochem. 267*, 2581−2587.
22. Aasa, R., and Vanngard, T. (1975) *J. Magn. Reson. 19*, 308−315.
23. Munro A. W., Noble, M. A., Robledo, L., Daff, S. N., and Chapman, S. K. (2001) Determination of the redox properties of human NADPH−cytochrome P450 reductase, *Biochemistry 40*, 1956−1963.
24. Dutton, P. L. (1978) Redox potentiometry: Determination of midpoint potentials of oxidation−reduction components of biological electron-transfer systems, *Methods Enzymol. 54*, 411−435.
25. Ost, T. W. B., Miles, C. S., Munro, A. W., Murdoch, J., Reid, G. A., and Chapman, S. K. (2001) Phenylalanine 393 exerts thermodynamic control over the heme of flavocytochrome P450 μ_B3, *Biochemistry 40*, 13421−13429.
26. Daff, S., Chapman, S. K., Turner, K. L., Holt, R. A., Govindaraj, S., Poulos, T. L., and Munro, A. W. (1997) Redox control of the catalytic cycle of flavocytochrome P450 μ_B3, *Biochemistry 36*, 13816−13823.
27. Southan M. D., Truscott, R. J. W., Jamie J. F., Pelosi L., Walker M. J., Maeda H., Iwamoto Y., and Tone S. (1996) Structural requirements of the competitive binding site of recombinant human indoleamine 2,3-dioxygenase, *Med. Chem. Res.* 343−352.
28. Seward, H. E. (1999) Magneto-optical spectroscopy of heme proteins, Ph.D. Thesis, University of East Anglia, Norwich, U.K.
29. Sono, M., and Dawson, J. H. (1984) Extensive studies of the heme coordination structure of indoleamine 2,3-dioxygenase and of tryptophan binding with magnetic and natural circular dichroism and electron paramagnetic resonance spectroscopy, *Biochim. Biophys. Acta 789*, 170−187.
30. Uchida, K., Shimizu, T., Makino, R., Sakaguchi, K., Iizuka, T., Ishimura, Y., Nozawa, T., and Hatano, M. (1983) Magnetic and natural circular dichroism of L-tryptophan 2,3-tryptophan dioxygenases and indoleamine 2,3-dioxygenase, *J. Biol. Chem. 258*, 2526−2533.
31. Cheesman, M. R., Greenwood, C., and Thomson, A. J. (1991) *Adv. Inorg. Chem. 36*, 201−255.
32. McKnight, J., Cheesman, M. R., Thomson, A. J., Miles, J. S., and Munro, A. W. (1993) Identification of charge-transfer transitions in the optical spectrum of low-spin ferric cytochrome P450 *Bacillus megaterium*, *Eur. J. Biochem. 213*, 683−687.
33. Gadsby, P. M. A., and Thomson, A. J. (1990) *J. Am. Chem. Soc. 112*, 5003.
34. Watmough, N. J., Cheesman, M. R., Butler, C. S., Little, R. H., Greenwood, C., and Thomson, A. J. (1998) The dinuclear center of cytochrome bo_3 from *Escherichia coli*, *J. Bioenerg. Biomembr. 30*, 55−62.
35. Terentis, A. C., Thomas, S. R., Takikawa, O., Littlejohn, T. K., Truscott, R. J. W., Armstrong, R. S., Yeh, S., and Stocker, R. (2002) The heme environment of recombinant human indoleamine 2,3-dioxygenase—Structural properties and substrate-ligand interactions, *J. Biol. Chem. 277*, 15788−15794.
36. Patel, N., Seward, H. E., Svensson, A., Gurman, S. J., Thomson, A. J., and Raven, E. L. (2003) *Arch. Biochem. Biophys. 418*, 197−204.
37. Eglinton, D. G., Gadsby, P. M. A., Sievers, G., Peterson, J., and Thomson, A. J. (1983) A comparative study of the low-temperature magnetic circular dichroism spectra of horse heart metmyoglobin and bovine liver catalase derivatives, *Biochim. Biophys. Acta 742*, 648−658.
38. Foote, N., Gadsby, P. M. A., Berry, M. J., Greenwood, C., and Thomson, A. J. (1987) *Biochem. J. 246*, 659−668.
39. Kobayashi, N., Nozawa, T., and Hatano, M. (1977) Magnetic circular dichroism studies on acid and alkaline forms of horseradish peroxidase, *Biochim. Biophys. Acta 493*, 340−351.
40. Bolard, J., and Garnier, A. (1972) *Biochim. Biophys. Acta 263*, 535−549.
41. Springall, J., Stillman, M. J., and Thomson, A. J. (1976) *Biochim. Biophys. Acta 453*, 494−501.
42. Nozawa, T., Kobayashi, N., and Hatano, M. (1976) *Biochim. Biophys. Acta 427*, 652−662.
43. Palmer, G. (1985) The electron paramagnetic resonance of metalloproteins, *Biochem. Soc. Trans. 13*, 548−560.
44. More, C., Belle, V., Asso, M., Fournel, A., Roger, G., Guigliarelli, B., and Bertrand, P. (1999) EPR spectroscopy: A powerful technique for the structural and functional investigation of metalloproteins, *Biospectroscopy 5*, S3−S18.
45. Yonetani, T., and Anni, H. (1987) Yeast cytochrome *c* peroxidase. Coordination and spin states of heme prosthetic group, *J. Biol. Chem. 262*, 9547−9554.
46. Suzuki, T., Kawamichi, H., and Imai, K. (1998) A myoglobin evolved from indoleamine 2,3-dioxygenase, a tryptophan-degrading enzyme, *Comp. Biochem. Physiol., Part B: Biochem. Mol. Biol. 121*, 117−128.
47. Newmyer, S. L., and Ortiz de Montellano, P. R. (1996) Rescue of the catalytic activity of an H42A mutant of horseradish peroxidase by exogenous imidazoles, *J. Biol. Chem. 271*, 14891−14896.
48. Yamazaki, F., Kuroiwa, T., Takikawa, O., and Kido, R. (1985) Human indoleamine 2,3-dioxygenase, *Biochem. J. 230*, 635−638.
49. Aitken, J. B., Thomas, S. E., Stocker, R., Thomas, S. R., Takikawa, O., Armstrong, R. S., and Lay, P. A. (2004) Determination of the nature of the heme environment in nitrosyl indoleamine 2,3-dioxygenase using mutiple-scattering analyses of X-ray absorption fime structure, *Biochemistry 43*, 4892−4898.
50. Jones, D. K., Patel, N. P., Cheesman, M. R., Thomson, A. J., and Raven, E. L. (2002) Leghaemoglobin: A model for the investigation of haem protein axial ligation, *Inorg. Chim. Acta 331*, 303−309.
51. Rosell, F. I., Ferrer, J. C., and Mauk, A. G. (1998) Proton-linked protein conformation swithcing: Definition of the alkaline conformation transition of yeast iso-1-ferricytochrome *c*, *J. Am. Chem. Soc. 120*, 11234−11245.
52. Makino, R., Sakaguchi, K., Iizuka, T., and Ishimura, Y. (1980) Acid−alkaline transition and thermal spin equilibirum of the heme in ferric L-tryptophan 2,3-dioxygenase, *J. Biol. Chem. 255*, 11883−11891.
53. Jones, D. K., Badii, R., Rosell, F. I., and Lloyd, E. (1998) Bacterial expression and spectroscopic characterization of soybean leghaemoglobin *a*, *Biochem. J. 330*, 983−988.
54. Foshay, M. C., Vitello, L. B., and Erman, J. E. (2004) pH dependence of heme iron coordination, hydrogen peroxide reactivity, and cyanide binding in cytochrome *c* peroxidase (H52K), *Biochemistry 43*, 5065−5072.
55. Turano, P., Ferrer, J. C., Cheesman, M. R., Thomson, A. J., Banci, L., Bertini, I., and Mauk, A. G. (1995) pH, electrolyte, and substrate-linked variations in active site structure of the Trp51Ala variant of cytochrome *c* peroxidase, *Biochemistry 34*, 13895−13905.
56. Raven, E. L., and Mauk, A. G. (2001) Chemical reactivity of the active site of myoglobin, *Adv. Inorg. Chem. 51*, 1−49.
57. Conroy, C. W., Tyma, P., Daum, P. H., and Erman, J. E. (1978) Oxidation−reduction potential measurements of cytochrome *c* peroxidase and pH dependent spectral transitions in the ferrous enzyme, *Biochim. Biophys. Acta 537*, 62−69.
58. Goodin, D. B., and McRee, D. E. (1993) The Asp−His−Fe triad of cytochrome *c* peroxidase controls the reduction potential, electronic structure, and coupling of the tryptophan free radical to the heme, *Biochemistry 32*, 3313−3324.
59. Harbury, H. A. (1957) Oxidation−reduction potentials of horseradish peroxidase, *J. Biol. Chem. 225*, 1009−1024.

60. Millis, C. D., Cai, D., Stankovich, M. T., and Tien, M. (1989) Oxidation−reduction potentials and ionization states of extracellular peroxidases from the lignin-degrading fungus *Phanerochaete crysoporium*, *Biochemistry 28*, 8484−8489.
61. Jones, D. K., Dalton, D. A., Rosell, F. I., and Raven, E. L. (1998) Class I heme peroxidases: Characterisation of soybean ascorbate peroxidase, *Arch. Biochem. Biophys. 360*, 173−178.
62. Tanaka, M., Ishimori, K., and Morishima, I. (1998) Structural roles of the highly conserved Glu residue in the heme distal site of peroxidases, *Biochemistry 37*, 2629−2638.
63. Yamada, H., Makino, R., and Yamazaki, I. (1975) Effrects of 2,4-substituents of deuteroheme upon redox potentials of horseradish peroxidases, *Arch. Biochem. Biophys. 169*, 344−353.
64. Sligar, S. G. (1976) Coupling of spin, substrate, and redox equilibria in cytochrome P450, *Biochemistry 15*, 5399−5406.
65. Cheesman, M. R., Watmough, N. J., Gennis, R. B., Greenwood, C., and Thomson, A. J. (1994) Magnetic-circular-dichroism studies of *Escherichia coli* cytochrome *bo*. Identification of high-spin ferric, low-spin ferric, and ferryl (Fe^{IV}) forms of heme *o*, *Eur. J. Biochem. 219*, 595−602.
66. Yagil, G. (1967) The proton dissociation constant of pyrrole, indole, and related compounds, *Tetrahedron 23*, 2855−2861.
67. Andonovski, B. S. (1999) UV study of the protonation of indole-2-carboxylic acid, 3-methylindole, 3-acetylindole, and D-tryptophan in perchloric acid solutions, *Croat. Chem. Acta 72*, 711−726.

BI0513958